Boundary fluctuation dynamics of a phase-separated domain in planar geometry

Nicolas Destainville and Nelly Coulonges

Laboratoire de Physique Théorique, Université de Toulouse, CNRS, UPS, Toulouse, France

Using phase-ordering kinetics and of renormalization group theories, we derive analytically the relaxation times of the long wavelength fluctuations of a phase-separated domain boundary in the vicinity of (and below) the critical temperature in the planar Ising universality class. For a conserved order parameter, the relaxation time grows like Λ^3 at wavelength Λ and can be expressed in terms of parameters relevant at the microscopic scale: lattice spacing, bulk diffusion coefficient of the minority phase, and temperature. These results are supported by numerical simulations of 2D Ising models, enabling in addition calculating the nonuniversal numerical prefactor. We discuss the applications of these findings to the determination of the real timescale associated with elementary Monte Carlo moves from the measurement of long wavelength relaxation times on experimental systems or molecular dynamics simulations.

I. INTRODUCTION

Phase separation phenomena are ubiquitous in nature, and many of them are observed in two dimensions, on surfaces, interfaces, or membranes [1,2]. When they belong to the Ising universality class [3,4], they are often numerically tackled with the help of this Ising model on a square or a triangular lattice. Beyond the original issues in magnetism and critical phenomena physics that motivated its intensive exploration during the 20th century [5], the Ising model and its extensions remain helpful to describe a wide range of phenomena in modern physics [6,7] and its applications. Applications go far beyond condensed matter physics, from the description of cell membranes [8] or animal skin patterning [9], to embryogenesis [10], and even to the dynamical description of geographical patterns [11], to name a few. In most cases, using the Ising model supposes having coarse grained a more complex original system, and one is in fact dealing with a mesoscopic model where microscopic degrees of freedom have been integrated out. In particular, simulating a mesoscopic, effective model enables one to save a considerable amount of computational time by avoiding dealing with microscopic details. Then this Ising model can be coupled to any mesoscopic model of interest, for example, a deformable membrane [8].

Below the critical temperature, binary mixtures exhibit fluctuating boundaries between separated phases, and determining the Ising parameter J from the spectral density of their fluctuations follows a well-established procedure. When the parameter J is just above its critical value, J_c, or equivalently said when the temperature T is close enough to the critical one, T_c, the underlying lattice has a limited importance only, and one recovers at large, macroscopic length scales the features of a continuous theory, notably the isotropy of the original experimental system. For example, a droplet of the minority phase then has a globally roundish shape [12,13], up to thermal fluctuations. The continuous limit will be extensively used in this work.

In the examples of applications given above, dynamical issues are generally at stake. An issue arises when one is interested in simulating the dynamics of the systems under study, because timescales of the real system and of the numerical model must be precisely related. This is at the core of kinetic Monte Carlo approaches relying on Monte Carlo local moves endowed with realistic dynamics [14]. Here we address this issue by calculating analytically the relaxation times of the fluctuation modes of a thermally activated boundary between phases in different geometries of interest. We use the exact analogy between lattice gases and conserved-order magnetic systems, and we follow the presentation of Bray [15] (here in two dimensions). Our main contribution is to carefully take into account the renormalization of the different quantities entering the relaxation times close to T_c. In particular, the spontaneous magnetization and the magnetic susceptibility have nontrivial behaviors, described by universal critical exponents. However, due to the hyperscaling relation between these different critical exponents, we end with a remarkably simple expression of the relaxation times. At the end of the calculation, we use numerical simulations on the very simple Ising model to estimate the numerical prefactors, which are not universal and cannot be derived from renormalization group considerations. This answers the initial question by relating explicitly the dynamics of the Ising model at the scale of local moves to the one of the interface fluctuation modes at large scales. The latter can in principle be measured either on experimental systems [16] or on molecular dynamics (MD) simulations [17]. Then one has access through our results to the real timescale associated with local moves, to be implemented in the numerical mesoscopic models of interest.

II. STRIPE GEOMETRY AND SQUARE AND TRIANGULAR LATTICES

We consider an Ising model [5] on a square lattice of lattice spacing a. The Ising variables (also usually called "spins") are

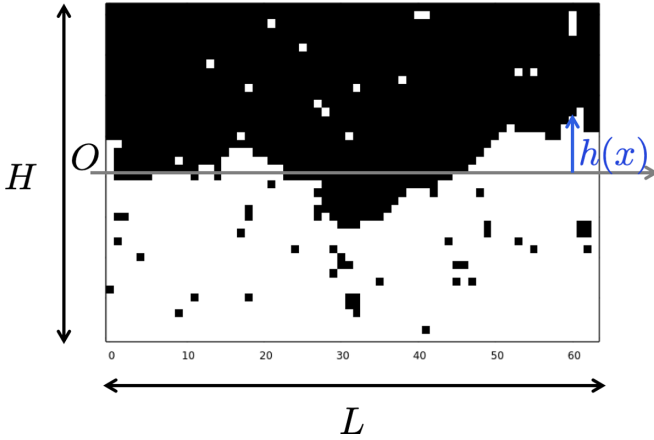FIG. 1. Snapshot of Monte Carlo simulation of the Ising model in equilibrium on a $L = 64$-long stripe at $T = 1.8J/k_B$. White (resp. black) squares represent $s_i = -1$ (resp. $+1$) Ising variables. The simulation box height is $H = 44$. The height function $h(x)$ encoding the position of the interface between both phases is also shown in blue. Far from the interface, i.e., in the bulk, both phases coincide with the two equilibrium ones minimizing the free energy defined below.

$s_i = \pm 1$, and the coupling is denoted by $J > 0$. The critical temperature is [18]

$$T_c = \frac{2}{\ln(1 + \sqrt{2})} \frac{J}{k_B} \simeq 2.27 \frac{J}{k_B}. \tag{1}$$

The first system of interest is a stripe of length L and height H, as shown in Fig. 1, at 0 total "magnetization" $\sum_i s_i$, so that there are exactly as many $+1$ and -1 Ising variables. The stripe height H is sufficiently large so that the boundary hardly ever hits the stripe upper or lower sides ($H \gg \sqrt{L}$).[1] Boundary conditions are set to -1 (resp. $+1$) on the lower (resp. upper) side, and are periodic between the vertical sides. Thus the height function $h(x)$, giving the position of the interface (or domain wall) between both phases, is L-periodic.

We denote by $\hat{h}_k(t)$ the Fourier coefficients of $h(x, t)$, $k \in \mathbb{Z}$:

$$\hat{h}_k(t) = \frac{1}{L} \int_0^L h(x, t) e^{-2i\pi kx/L} \, dx. \tag{2}$$

The associated wavelength is $\Lambda = L/|k|$ for $k \neq 0$. We assume without loss of generality that $h(x)$ fluctuates around 0, that is to say, $h_0 = \langle h(x, t) \rangle = 0$ by choosing properly the origin of the ordinates.

We recall that in reality the interface has a finite width in the y direction, set by the correlation length ξ. At a distance much larger than ξ from the interface, bulk phases coincide with the two equilibrium ones minimizing the free energy defined below.

_____

[1]The height fluctuations $\sqrt{\langle h^2 \rangle} \propto \sqrt{L}$ for an interface with line tension λ, using, for example, Eq. (25) and summing over modes k. Hence $\sqrt{\langle h^2 \rangle} \ll H$. Consequently the interface hardly ever hits the upper or lower sides, as observed in practice in the simulations.

A. Continuous limit

We will adopt below a continuous field-theoretic approach where the discrete Ising variables $s_i = \pm 1$ become a continuous, coarse-grained real field $\phi(\mathbf{r}) \in [-1, 1]$, the local average of the s_i, governed by the Landau-Ginzburg free-energy functional [5,15]

$$F[\phi] = \int d^2\mathbf{r} \left[\frac{1}{2} (\nabla \phi)^2 + V(\phi) \right]. \tag{3}$$

In this relation, $V(\phi) = \frac{r}{2} \phi^2 + u\phi^4$ is a potential energy that, below the critical temperature T_c, favors the coexistence of two phases because $r < 0$. At very low temperature, the two stable phases correspond to $\phi_+ = 1$ and $\phi_- = -1$, i.e., pure $+1$ and pure -1 phases. However, thermal agitation brings some disorder, so that ϕ_+ and ϕ_- get closer when T grows and eventually become very close when reaching the critical temperature T_c.

A very useful quantity below is the chemical potential defined by the functional derivative of $F[\phi]$:

$$\mu(\mathbf{r}) = \frac{\delta F}{\delta \phi}. \tag{4}$$

It is shown in Ref. [15] that the bulk concentration relaxes much faster than the interface does when the order parameter is conserved, so that the concentration field ϕ obeys Laplace's equation $\nabla^2 \phi = 0$ in the bulk at the timescales of interest. It ensues that μ depends linearly on ϕ in the bulk, and thus that μ also obeys Laplace's equation $\nabla^2 \mu = 0$ there.

We wish to emphasize here that in principle the order parameter ϕ represents the magnetization field in the original Landau-Ginzburg theory; however, it can also be considered as a local concentration after some basic algebraic manipulation: the field $\phi \in [-1, 1]$, so that $c = (\phi + 1)/2 \in [0, 1]$ is the local fraction of one species and $1 - c$ the local fraction of the other species if the Ising model is seen as a lattice gas, where -1 and $+1$ spins now represent two coexisting species (such as two atomic species in a binary alloy). Both quantities, magnetization and concentration, are equivalent. By extension, we shall generally use below the lattice-gas vocabulary, even though ϕ and c do not exactly coincide. Notably, the chemical potential μ would correspond to the external magnetic field in the magnetism vocabulary.

The continuous limit is valid provided that $\xi/a \gg 1$. In other words, the temperature $T < T_c$ must be close enough to T_c. More precisely [18]

$$\frac{\xi}{a} \simeq \frac{k_B T}{4J} \left(1 - \frac{T}{T_c} \right)^{-1} \tag{5}$$

for the 2D Ising model on a square lattice, which sets the regime of temperature for which the condition $\xi/a \gg 1$ is fulfilled (in general, the behavior of ξ is governed by the critical exponent ν [5], equal to 1 in the present case). We also recall that a line tension, denoted by λ, is associated with the interface because it bears an energy cost proportional to its length. Thus λ has the dimension of a force. As discussed below, it vanishes close to the critical point.

B. Evolution equation and relaxation times

We consider a single mode $k > 0$ of interface fluctuation, i.e., $h(x, t = 0) = \alpha_0 \cos(qx)$ with $q = 2k\pi/L = 2\pi/\Lambda$. We suppose that α_0 is small, i.e., much smaller than all relevant length scales apart from a. In particular, $\alpha_0 \ll \Lambda$, so that we work in the small gradient approximation, $|h'(x)| \ll 1$.

We neglect the thermal noise in the interface dynamics, so that it will spontaneously return to its equilibrium position $h = 0$, driven by the line tension λ: $h(x, t)$ is expected to be of the form $h(x, t) = \alpha_0 \cos(qx)e^{-t/\tau_q}$ for $t > 0$.[2] Langevin theory asserts that the relaxation time τ_q that we will determine below is equal to the decay time of the temporal correlation function of the Fourier coefficient that we shall measure in the presence of thermal fluctuations and thus in numerical simulations.

Following Bray [15], section 2.4, one writes the evolution equation of $h(x, t)$ by calculating the interface velocity v in the y direction. We first need to compute the chemical potential $\mu(x, y, t)$. It satisfies Laplace's equation $\nabla^2 \mu = 0$ far from the interface (see above), and it is subject to the Gibbs-Thomson-like boundary condition at the 1D interface [see Eq. (28) of Ref. [15]]:

$$\mu(x, h(x), t) = -\frac{\lambda K(x)}{\Delta \phi}. \tag{6}$$

Here $\Delta \phi = \phi_+ - \phi_-$ is the difference of concentrations between both bulk phases (see below) and $K(x)$ is the local interface curvature. Introducing the vector $\hat{\mathbf{g}} = (g_x, g_y)$ normal to the interface [15], we see

$$K(x) = \frac{dg_x}{dx} = -\frac{h''(x)}{[1 + h'(x)^2]^{3/2}} \simeq -h''(x) = q^2 h(x). \tag{7}$$

In addition, since α_0 is assumed to be small, we can set $h(x) = 0$ in the left-hand side of Eq. (6), which now reads

$$\mu(x, 0, t) = -\frac{\lambda q^2 h(x, t)}{\Delta \phi}. \tag{8}$$

We naturally assume μ to be of the form $\mu(x, y, t) = \cos(qx)f(y)e^{-t/\tau_q}$ in the bulk, so that Laplace's equation leads to

$$f''(y) - q^2 f(y) = 0. \tag{9}$$

Since μ cannot diverge at $\pm\infty$, the only physical solution is $f(y) = Ae^{-q|y|}$.

With the boundary condition, one eventually gets the chemical potential in the whole plane:

$$\mu(x, y, t) = -\frac{\lambda \alpha_0}{\Delta \phi} q^2 \cos(qx)e^{-q|y|}e^{-t/\tau_q}. \tag{10}$$

We can now infer the interface velocity v from μ by using the Eq. (29) of Ref. [15], $v\Delta\phi = -\Gamma[\frac{\partial \mu}{\partial y}]_{-\epsilon}^{\epsilon}$, where the square brackets indicate the discontinuity across the interface. Indeed, the interface moves because of the imbalance between the currents flowing into and out of it, themselves proportional

to the gradient of μ perpendicularly to the interface, $\frac{\partial \mu}{\partial y}$. Here we have reintroduced a transport coefficient Γ that is implicit in Bray, being "adsorbed into the timescale" [15]; Γ^{-1} is homogeneous to a drag coefficient per unit area, arising from the continuity equation [below Bray's Eq. (3), noted λ therein]. We have also identified Bray's normal coordinate g with y in the small-gradient approximation. It follows that

$$v(x, t) = -\frac{2\Gamma\lambda\alpha_0}{(\Delta\phi)^2} q^3 \cos(qx)e^{-t/\tau_q} = -\frac{2\Gamma\lambda}{(\Delta\phi)^2} q^3 h(x, t) \tag{11}$$

because we have anticipated that $h(x, t) = \alpha_0 \cos(qx)e^{-t/\tau_q}$. Note the q^3 factor, coming from q^2 in μ and the derivative $\frac{\partial \mu}{\partial y}$. Now, by definition, $v = \frac{\partial h}{\partial t} = -\frac{1}{\tau_q} h(x, t)$. It follows that

$$\tau_q = \frac{(\Delta\phi)^2}{2\Gamma\lambda q^3}. \tag{12}$$

Far below T_c, $\phi_\pm = \pm 1$ so that $\Delta\phi \simeq 2$, while it decreases to 0 when T goes close to T_c as discussed above. We shall return to this point below.

C. Introduction of the bulk diffusion coefficient

We now relate the transport coefficient Γ to the bulk diffusion coefficient D in each phase. We start from the evolution equation governing the time evolution of the (conserved) order parameter ϕ (model B or the Cahn-Hilliard equation) [5,15]:

$$\frac{\partial \phi}{\partial t} = \Gamma\nabla^2 \frac{\delta F}{\delta \phi}, \tag{13}$$

where we have also reintroduced the transport coefficient Γ implicit in Bray. Here $F[\phi]$ is again the free-energy functional of Eq. (3) with $V(\phi)$ the potential energy of the Landau-Ginzburg theory [5]. In the bulk, if we now assume small perturbations of ϕ close to ϕ_+ (or equivalently ϕ_-) so that we can write $\phi = \phi_+ + \tilde{\phi}$, Eq. (13) becomes the diffusion equation [see below Bray's Eq. (21)]:

$$\frac{\partial \tilde{\phi}}{\partial t} = \Gamma V''(\phi_+)\nabla^2 \tilde{\phi}. \tag{14}$$

Below T_c, $V(\phi)$ has two minima $\phi = \phi_\pm$. We assume for simplicity that $\phi_- = -\phi_+$, $V(\phi_+) = V(\phi_-)$, and $V''(\phi_+) = V''(\phi_-)$ because both bulk phases play the same role [15]. Hence one can identify $\Gamma V''(\phi_+)$ with the diffusion coefficient in the bulk D, so that Eq. (12) becomes

$$\tau_q = \frac{V''(\phi_+)(\Delta\phi)^2}{2D\lambda q^3}. \tag{15}$$

The line tension λ being the driving force of the interface relaxation, τ_q naturally appears to be inversely proportional to λ in this expression. It directly ensues from Eq. (13), even though λ is not the only factor to depend on T in this relation as we shall see now.

D. Vicinity of the critical temperature

Now we determine how the factor $V''(\phi_+)(\Delta\phi)^2$ depends on the temperature close to T_c. We introduce the reduced temperature $\theta = T/T_c < 1$. First, $\Delta\phi$ is twice the bulk concentration close to T_c. Thus, $\Delta\phi \propto (1 - \theta)^\beta$, where we have

---

[2]Anticipating the exponential time dependence of $h(x, t)$ is not a prerequisite. Alternatively, one can just anticipate any factor $\ell(t)$ that would satisfy a first-order ODE at the end of the calculation.

used the definition of the critical exponent β [5]. Second, in the bulk, ϕ is uniform, thus the chemical potential in Eq. (4) is also uniform and reads $\mu = \delta F/\delta\phi = V'(\phi) - \nabla^2\phi$. As already discussed, the last term is negligible in the bulk because ϕ obeys Laplace's equation at the timescales of interest [15] and

$$V''(\phi_+) = \frac{d\mu}{d\phi}(\phi = \phi_+) \tag{16}$$

$$= \frac{1}{\frac{d\phi}{d\mu}(\mu = 0)} \tag{17}$$

$$= \frac{1}{\chi(\mu = 0)} \tag{18}$$

$$\propto (1-\theta)^\gamma, \tag{19}$$

where χ is the (magnetic) susceptibility and γ the associated critical exponent. Indeed, using the previously mentioned analogy between the chemical potential μ (resp. the concentration ϕ) and an external magnetic field, h (resp. magnetization m), we used the definition of the magnetic susceptibility $\chi = (\frac{\partial m}{\partial h})_T (h = 0)$ [18]. To go from the second to the third line above, we assumed that $\mu(\phi)$ is locally bijective in the neighborhood of ϕ_+, and we used that $\mu(\phi_+) = 0$ since $\phi = \phi_+$ (or ϕ_-) at vanishing μ. It follows that $V''(\phi_+)(\Delta\phi)^2 \propto (1-\theta)^{2\beta+\gamma} = (1-\theta)^2$ owing to the hyperscaling relation between critical exponents [5] $2\beta + \gamma = d\nu$, in dimension $d = 2$ where $\nu = 1$ for the Ising model [18]. The final behavior of $V''(\phi_+)(\Delta\phi)^2$ is remarkably simple.

Beyond this scaling law, we are interested in the prefactors: $\Delta\phi$ has no dimension and V'' is proportional to J/a^2. Indeed, $J \propto k_B T_c$ is the only energy scale in the problem close to T_c and there is one Ising variable per elementary square of area a^2 (see Ref. [8] for details). Hence

$$\tau(\Lambda) = \text{const}\frac{J}{a^2 D\lambda}\Lambda^3(1-\theta)^2, \tag{20}$$

where we have written the relaxation time in function of the wavelength $\Lambda = 2\pi/q$ and const is a numerical constant. Contrary to the critical exponents, this prefactor is not universal; it depends on the microscopic details such as the underlying lattice.

Furthermore $\lambda = 4(1-\theta)J/a$ at first order in $1-\theta$ [12], in other words, $1 - \theta = \frac{1}{4}\lambda a/J$. Injecting this relation in the expression of $\tau(\Lambda)$, we get the simpler alternative expression

$$\tau(\Lambda) = A\frac{\lambda}{DJ}\Lambda^3, \tag{21}$$

where A is a numerical constant, again nonuniversal. This is our main result: once the constant A has been benchmarked on well-defined numerical systems (see below), the measure of $\tau(\Lambda)$ on experimental systems or MD simulations enables one to infer the bulk diffusion coefficient D in real time units.

This dependence of the timescale on the cube of the length scale, $\tau(\Lambda) \propto \Lambda^3$, is reminiscent of the law governing the coarsening of the same Ising model with conserved order parameter after a quench from high to low temperature [15]. In the latter case, the relaxation time of a length scale L also grows proportionally to L^3. Both mechanisms are closely related.

Remark 1: In principle, the diffusion coefficient D also depends on the temperature T. First, quantifying how (out-of-equilibrium) concentration fluctuations relax, as expressed by Eq. (14), D is a *cooperative* diffusion coefficient (also called a *mutual* or *collective* or *gradient* diffusion coefficient), to be contrasted with the *self*-diffusion coefficient describing the evolution of a single tagged particle [5,19]. Note that both coincide in the limit of small density fluctuations. Critical phenomena theory states that D goes to zero close to the critical point, which is related to critical slowing down. This is characterized by a dynamic critical exponent z relating the correlation length ξ and the correlation time τ through $\tau \sim \xi^z$ close to criticality. The diffusion coefficient then behaves like $D \sim \xi^2/\tau$ close to T_c [20], i.e. (see also Ref. [21])

$$D \sim \xi^{2-z} \propto (1-\theta)^{z'} \tag{22}$$

with $z' = -\nu(2-z) = -(2-z)$ in the present case according to Eq. (5). If we specialize this result to the present Ising model with conserved order parameter (model B), a commonly accepted value is $z = 4 - \eta$ where η is another critical exponent equal to $1/4$ in the present case [5], leading to $z' = 7/4$ (see Ref. [20] for recent numerical verification).

In practice, however, when going away from the critical point, D goes to a finite value D_0. Then the inverse diffusion coefficient can be interpolated by

$$D^{-1} \simeq D_0^{-1} + C(1-\theta)^{-z'} \tag{23}$$

as proposed in Ref. [22], where C is a model-dependent parameter that can be measured, from simulations or experiments. From now, we assume that D_0 dominates rapidly when one goes away from T_c, in particular for the values θ studied here, as observed experimentally in Ref. [22], and we write $D \simeq D_0$.

Remark 2: In the Ising model of interest here, on a lattice with lattice spacing a, let us denote by δt the (simulation) time step associated with local flips. Then $D = D_0 = a^2/(4\delta t)$ for a freely bulk-diffusing single spin in a sea of opposite spins, i.e., at low enough density fluctuations.

Also using that $\lambda = 4(1-\theta)J/a$, we can then also write

$$\frac{\tau(\Lambda)}{\delta t} = A'(1-\theta)\left(\frac{\Lambda}{a}\right)^3. \tag{24}$$

One expects A and $A' = 16A$ to be slowly varying functions of θ close to T_c, since the singularities are captured by the critical exponents.

III. MONTE CARLO SIMULATION RESULTS IN STRIPE GEOMETRY

We begin with simulations on the square lattice with Kawasaki dynamics, at conserved order parameter [14]. In practice, one must be as close as possible to T_c to use the scaling relations, as well as to use the continuous approach described above; however, close to T_c, the small-gradient approximation fails to describe the interface. A compromise must be found and we focus on the temperature range $\theta = 0.6$ to 0.8. A simulation snapshot is given in Fig. 1 at $\theta = 0.79$, i.e., $T = 1.8J/k_B$. We have focused here on a relatively small system, $L = 64$ and $H = 44$, in order to have good statistical

TABLE I. Theoretically predicted and numerically measured line tensions for $L = 64$ and 128-long stripes (square lattice) in function of the reduced temperature $\theta = T/T_c$ and in units of J/a. The duration of each simulation is 10^{12} and 12×10^{12} for $L = 128$) Monte Carlo steps. Error bars are 68% confidence intervals.

T/T_c	λ_{theo}	$\lambda_{\text{num},64}$	$\lambda_{\text{num},128}$
0.61	1.53	1.49 ± 0.11	
0.70	1.18	1.16 ± 0.05	1.14 ± 0.07
0.79	0.83	0.79 ± 0.03	

sampling. However, finite-size effects can affect the measurements of some thermodynamic quantities, such as the apparent localization of the critical temperature, or the apparent critical exponents. This has been thoroughly explored in the past [14]. Here the principal limitation comes from the fact that the accessible wavelengths L/k, k integer must be much larger than 1, so that the continuous limit remains meaningful. To ascertain that our numerical findings are not affected by such effects, we have performed a longer run on one larger 128×65 system, as detailed below. Simulation durations were chosen so that more than 1000 statistically independent samples were computed for each condition (500 ones for $L = 128$). This number was obtained by taking into account the slowest relaxation mode ($k = 1$) of the phase boundary.

A. Line tension

We first extract the values of the line tension λ and check their consistence w.r.t. the theoretical predictions. Owing to the Equipartition Theorem in thermodynamic equilibrium, the fluctuation spectrum depends on the line tension as.[3]

$$\langle |\hat{h}_k|^2 \rangle = \frac{L k_B T}{4\pi^2 \lambda k^2}. \tag{25}$$

In practice, we regularly measure the height function $h(x, t)$ as follows. Confusion between the interface and small bubbles must be avoided (see Fig. 1), all the more so as such bubbles become more probable when getting close to the transition. For each abscissa $x \in [1, L]$, starting from the bottom of the simulation box where -1 spins are the majority, we progress upward until we encounter a series of four consecutive $+1$ spins or more, or alternatively we reach the upper side (which is highly improbable because $H \gg \sqrt{L}$). This numerically defines $h(x)$, in units of the lattice spacing a. The choice of four consecutive spins above comes from the fact that for the temperatures studied here, we have observed bubbles of this size in the bulk phases to be very rare (see Fig. 1). We have checked by visual inspection that this procedure faithfully captures the domain boundary for the range of temperature studied in this work.

---

[3]This relation ensues from the Equipartition Theorem [5] after writing in the Fourier space the interface energy $\frac{\lambda}{2} \int_0^L |h'(x)|^2 \, dx$ in the small-gradient approximation (see, for example, Ref. [16] for the calculation in a similar context)

Then we compute the Fourier coefficients $\hat{h}_k(t)$ with a fast Fourier transform (FFT) routine, and then average $|\hat{h}_k|^2$ over simulation time. The values given below are obtained by fitting the three first modes, $k = 1$ to 3. In Table I these numerical values are compared to the (asymptotically exact) theoretical ones close to T_c, i.e., $\lambda = 4(1 - \theta)J/a$. The agreement is good in spite of the diverse approximations used, such as the small gradient approximation or the above asymptotic behavior of λ close to the critical point.

Remark: To check the validity of the small gradient approximation, one can estimate the order of magnitude of the gradient $\partial h/\partial x$. Owing to the discrete version of Parseval's identity, the average value of $|\partial h/\partial x|^2$ is computed as follows:

$$\left\langle \frac{1}{L} \int_0^L \left| \frac{\partial h}{\partial x} \right|^2 dx \right\rangle = \sum_k q_k^2 \langle |\hat{h}_k|^2 \rangle \tag{26}$$

$$= \sum_{k=0}^{L/a-1} \left(\frac{2k\pi}{L} \right)^2 \frac{L k_B T}{4\pi^2 \lambda k^2} \tag{27}$$

$$= \frac{k_B T}{a\lambda}. \tag{28}$$

All modes contribute equally. Here owing to Table I, $\lambda \approx J/a = \frac{\ln(1+\sqrt{2})}{2} k_B T_c/a$. Thus $\frac{k_B T}{a\lambda} \approx \frac{2}{\ln(1+\sqrt{2})} \frac{T}{T_c}$. It follows that $\partial h/\partial x$ is already of order 1 with the temperatures studied here, and one cannot reasonably go closer to T_c, where λ would tend to zero and the gradient diverge.

B. Relaxation times

Once line tensions have been determined, we can use Eq. (21) to calculate the value of the numerical constant A. In the simulation units, $D = 1/4$, implicitly in units of a^2 per Monte Carlo sweep of duration δt [14]. In practice, for a fixed mode k (or $q = 2k\pi/L$), to compute τ_k, the coefficients $\hat{h}_k(t)$ are Fourier transformed with respect to time (again with the help of FFT), the new Fourier coefficients being denoted by $\tilde{h}_k(\omega)$. We are interested in the correlation function $\hat{C}_k(s) = \langle \hat{h}_k(t)\hat{h}_k^*(t+s) \rangle$, where the asterisk denotes the complex conjugate. Owing to Wiener-Khinchin's theorem one finally gets

$$\hat{C}_k(s) \propto \text{FT}^{-1}[|\tilde{h}_k(\omega)|^2](s), \tag{29}$$

where FT^{-1} is the inverse Fourier transform w.r.t. time, from which we can extract the relaxation time τ_k of each mode k by fitting $\hat{C}_k(s)$ in normal-log coordinates on its linear regime [23]. Figure 2 provides examples of measured relaxation times and illustrates that $\tau(\Lambda) \propto \Lambda^3$.

Using Eq. (21), and averaging the measured $\tau(\Lambda)/\Lambda^3$ over the three slowest modes, we eventually find $A \simeq 0.26$ for $\theta = 0.61$, $A \simeq 0.26$ for $\theta = 0.70$ (and $A \simeq 0.29$ if $L = 128$ at this temperature), and $A \simeq 0.32$ for $\theta = 0.79$ on the square lattice. The relative lack of accuracy on the value of A principally comes from two antagonistic constraints: the deviation from the small gradient approximation increases when T gets too close to T_c where λ vanishes, and by contrast, the first-order expansion of Eq. (21) is valid only close to T_c.
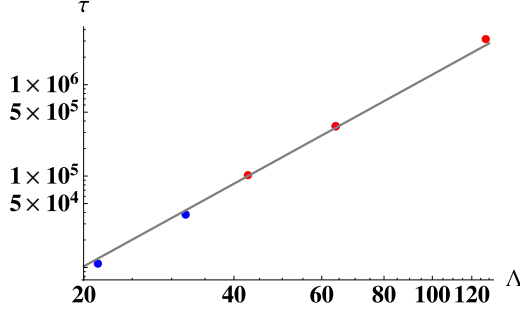
FIG. 2. Relaxation times (in units of δt) of the three slowest modes ($k = 1$ to 3) in function of the wavelength $\Lambda = L/k$ (in units of a), for the reduced temperature $\theta = 0.70$ and two system sizes $L = 64$ (blue dots) and $L = 128$ (red dots). The two points at $\Lambda = 64$ are almost superimposed. Log-log coordinates. The continuous line has slope 3 for comparison with the expected behavior of Eq. (21).

C. Triangular lattice

We now confront our analytical results to numerical ones on an alternative 2D lattice. We adapt the above simulation procedure to the triangular lattice. In addition to the N, S, W, and E edges of the square lattice, we add NW and SE ones so that each vertex in the bulk now has six nearest neighbors. The boundary conditions are unchanged as compared to the previous case.

The critical temperature becomes [18]

$$T_c = \frac{4}{\ln 3} \frac{J}{k_B} \simeq 3.64 \frac{J}{k_B}. \quad (30)$$

Some care must be taken of the definition of the height function with the chosen boundary conditions. Indeed, we detect the boundary along the sequence of spins parallel to the y axis, at fixed abscissa. The so-obtained height must then be rescaled by a geometrical factor $\sqrt{3}/2$ because the actual lattice unit cell is an equilateral triangle of height $\sqrt{3}a/2$ along the y axis. In Table II numerical values of the so-obtained line tension λ are again compared to the theoretical ones close to T_c, $\lambda = 4\sqrt{3}(1 - \theta)J/a$ on a triangular lattice [13], after following the same process as above. The agreement is almost as good as in the square lattice case.

Furthermore, using Eq. (21), and again averaging the measured $\tau(\Lambda)/\Lambda^3$ over the three slowest modes, we find on the triangular lattice $A \simeq 0.10$ for $\theta = 0.71$ and $A \simeq 0.12$ for $\theta = 0.77$. In this case, Eq. (24) still holds with $A' = 16\sqrt{3}A$. The value of A differs from the square-lattice one owing to the nonuniversal character of this prefactor.

TABLE II. Theoretically predicted and numerically measured line tensions for $L = 64$-long stripes (triangular lattice) in function of the reduced temperature $\theta = T/T_c$, in units of J/a. The duration of each simulation is 10^{12} Monte Carlo steps. Error bars are 68% confidence intervals.

T/T_c	λ_{theo}	λ_{num}
0.71	1.98	2.10 ± 0.08
0.77	1.60	1.73 ± 0.07

IV. CIRCULAR GEOMETRY AND POLAR COORDINATES

We now consider a quasicircular droplet of $+1$ spins in a sea of -1 spins. The droplet radius is $R_0 \gg a$ if it were perfectly circular, i.e., its (conserved) area is πR_0^2. We recall that for temperatures close enough to T_c, the isotropy of the system is restored at large length scales, independently of the lattice symmetries. We again perturb the circular droplet by considering only the mode k. Taking into account conservation of the order parameter is slightly more complex than in the stripe geometry above. If we set the origin at the center of the original circle, the boundary shape in polar coordinates reads $r(\theta) = R_0[1 + u_0 + u_k \cos(k\theta)] = r_0 + \rho_0 \cos(k\theta)$, considering again the mode k. Here $r_0 = R_0(1 + u_0)$ and $\rho_0 = R_0 u_k \ll r_0$. Indeed, one must keep the mode $k = 0$, u_0, because conservation of domain area imposes a relationship between the different modes u_k [16]. It follows that $r''(\theta) = k^2[r_0 - r(\theta)]$.

In polar coordinates, the curvature is given that

$$K = \frac{r(\theta)^2 + 2r'(\theta)^2 - r(\theta)r''(\theta)}{[r(\theta)^2 + r'(\theta)^2]^{3/2}} \simeq \frac{1}{r(\theta)} - \frac{r''(\theta)}{r^2(\theta)}$$

$$= \frac{1}{r(\theta)}(1 + k^2) - \frac{k^2 r_0}{r^2(\theta)} \quad (31)$$

in the small gradient approximation ($\rho_0 \ll r_0$) where $r'(\theta)$ and $r''(\theta) \ll r(\theta)$. At order 1, one also gets

$$\frac{1}{r(\theta)} = \frac{1}{r_0} - \frac{\rho_0}{r_0^2} \cos(k\theta), \quad (32)$$

and K becomes

$$K = \frac{1}{r_0}\left[1 + (k^2 - 1)\frac{\rho_0}{r_0}\cos(k\theta)\right]. \quad (33)$$

To determine the chemical potential μ in the whole plane, we use again the boundary condition $\mu(\theta, r(\theta), t) \simeq \mu(\theta, r_0, t) = -\frac{\tilde{\lambda}K(\theta)}{\Delta\phi}$. In polar coordinates, the Laplace equation $\nabla^2 \mu = 0$ reads

$$\frac{\partial^2 \mu}{\partial r^2} + \frac{1}{r}\frac{\partial \mu}{\partial r} + \frac{1}{r^2}\frac{\partial^2 \mu}{\partial \theta^2} = 0. \quad (34)$$

We first determine μ *outside* the domain, i.e., for $r > r_0$. We look for a solution of the form $\mu(\theta, r, t) = \mu_0(r) + f(r)\cos(k\theta)e^{-t/\tau_k}$, where $\mu_0(r) = -\frac{\lambda}{\Delta\phi}\frac{\ln r}{r_0 \ln r_0}$ is the solution in two dimensions in the absence of boundary fluctuations. It follows that

$$r^2 f''(r) + r f'(r) - k^2 f(r) = 0. \quad (35)$$

Looking for a power-law solution, $f(r) = Br^\alpha$, and injecting it in Eq. (35), we get

$$\alpha(\alpha - 1)Br^\alpha + \alpha Br^\alpha - k^2 Br^\alpha = (\alpha^2 - k^2)Br^\alpha = 0. \quad (36)$$

There are two independent solutions, $\alpha = \pm|k|$ for $|k| > 1$, and we choose $\alpha = -|k|$, the only solution remaining finite at infinity. The constant B is determined through the boundary condition $\mu(r_0, \theta) = -\frac{\lambda}{r_0 \Delta\phi} - (k^2 - 1)\frac{\sigma_0 \rho_0}{r_0^2}\cos(k\theta)$, we find

$B = \text{const } r_0^{|k|}$. Finally, for $r > r_0$,

$$\mu(\theta, r, t) = \frac{\lambda}{\Delta\phi} \left[-\frac{1}{r_0} \frac{\ln r}{\ln r_0} \right.$$
$$\left. + \frac{\rho_0}{r_0^2}(k^2 - 1)\left(\frac{r_0}{r}\right)^{|k|} \cos(k\theta) \right] e^{-t/\tau_k}. \quad (37)$$

Inside the domain, i.e., for $r < r_0$, the trivial solution in absence of fluctuations would be $\mu_0 = \text{const} = -\frac{\lambda}{r_0\Delta\phi}$. This time, we look for a solution being regular at the origin O, so that we keep only the solution $\alpha = +|k|$:

$$\mu(\theta, r, t) = \frac{\lambda}{\Delta\phi} \left[-\frac{1}{r_0} + \frac{\rho_0}{r_0^2}(k^2 - 1)\left(\frac{r}{r_0}\right)^{|k|} \cos(k\theta) \right] e^{-t/\tau_k}. \quad (38)$$

We look for the discontinuity at r_0:

$$r > r_0 : \frac{\partial\mu}{\partial r}(r_0 + \epsilon)$$
$$= \left[-\frac{\lambda}{r_0^2 \ln r_0 \Delta\phi} - \frac{\lambda\rho_0}{r_0^3 \Delta\phi}(|k|^3 - |k|) \cos(k\theta) \right] e^{-t/\tau_k}$$

$$r < r_0 : \frac{\partial\mu}{\partial r}(r_0 - \epsilon)$$
$$= \frac{\lambda\rho_0}{r_0^3 \Delta\phi}(|k|^3 - |k|) \cos(k\theta) e^{-t/\tau_k}, \quad (39)$$

where $\epsilon > 0$ is vanishingly small. The interface velocity $v(\theta, t)$ is now given by [15] $v\Delta\phi = -\Gamma[\frac{\partial\mu}{\partial r}]_{r_0-\epsilon}^{r_0+\epsilon}$. We are interested only in the contribution of v on the relaxation of mode k. Indeed, there is also a contribution acting on r_0 and making it go to 0 at large times. In standard coarsening theory, this expresses the evaporation of small domains to the benefit of largest ones, elsewhere in the system (Ostwald ripening) [15]. Here we are not interested in this very long timescale process because we consider a single isolated domain on shorter timescales. As $u_0 = O(u_k^2)$ [16], there is no coupling between modes 0 and k at order 1. Thus

$$v(\theta, t) = -2\frac{\lambda\Gamma\rho_0}{r_0^3(\Delta\phi)^2}(|k|^3 - |k|) \cos(k\theta) e^{-t/\tau_k}$$
$$= \frac{\partial r}{\partial t} = -\frac{1}{\tau_k} r(\theta, t) \quad (40)$$

leading to

$$\tau_k = \frac{r_0^3(\Delta\phi)^2}{2\Gamma\lambda} \frac{1}{|k|^3 - |k|}. \quad (41)$$

Note that $k = 1$ is a soft mode in polar geometry, corresponding to the translation of the domain center. Its relaxation time is thus irrelevant in this geometry.

The connection with the above Cartesian geometry can be done by identifying $q = k/r_0 = 2\pi k/L$, because the unperturbed interface length is $L = 2\pi r_0$. At large k, $|k|^3 - |k| \simeq |k|^3$ and we recover

$$\tau_k \simeq \frac{(\Delta\phi)^2}{2\Gamma\lambda q^3}, \quad (42)$$

as in Cartesian geometry [see Eq. (12)] because the interface is locally flat at the scale of the wavelength $\Lambda \ll R_0$. Also note

that the chemical potentials in polar and Cartesian geometries are equal close to the interface. Indeed, let us, for example, consider the neighborhood of the point $(0, r_0)$ of the interface and write $(x, y) = (0, r_0 + Y)$, where Y is the distance to the interface. If $r > r_0$, i.e., $Y > 0$, $(r_0/r)^k = \exp[-k\ln(1 + Y/r_0)] \simeq \exp(-qY)$ provided that we identify $q = k/r_0 = 2\pi k/L$, with $L \simeq 2\pi r_0$. In the same way $(r/r_0)^k \simeq \exp(qY)$ close to the interface if $r < r_0$, i.e., $Y < 0$.

To conclude, since the large k behavior is the same for stripe and circular geometries, it follows that the numerical prefactor A determined in stripe geometry above, depending on the underlying lattice, can also be used here to relate numerically the relaxation times to the model parameters, as follows:

$$\tau(\Lambda) = A \frac{\lambda}{DJ} \frac{\Lambda^3}{1 - \left(\frac{\Lambda}{2\pi r_0}\right)^2}. \quad (43)$$

This relation results from Eq. (41) by using the same calculation as above when deriving Eq. (21) from Eq. (12), but in circular geometry instead of stripe geometry.

V. DISCUSSION

We come back to the initial issue raised in the introduction: How to extract the real timescale associated with Kawasaki local moves from the measurement of macroscopic timescales of boundary relaxation modes? Assume that we can localize and track experimentally or in MD numerical simulations the interface between two phases, either in stripe or in polar (droplet) geometry. To gain computational efficiency and address larger system sizes on longer timescales, the system can be advantageously simulated with the help of the coarse-grained Ising model on a square or a triangular lattice (see, e.g., Ref. [8]) provided that (1) the Ising coupling J and (2) the time step δt associated with each Monte Carlo step are suitably chosen. They significantly depend on the choice of the lattice spacing a, which must be chosen to be smaller than all length scales of interest in the problem considered (except of course the molecular ones). We propose the following protocol to properly determine J and δt:

(1) Measure the line tension λ with the help of the interface fluctuation spectrum in equilibrium measured on real systems or MD simulations, as prescribed by Eq. (25) [16].

(2) T is set by the experimental conditions; thus J_c is given by $J_c = \frac{\ln(1+\sqrt{2})}{2}k_BT$ (resp. $\frac{\ln 3}{4}k_BT$) on a square (resp. triangular) lattice. Then J can be estimated close enough to J_c by known exact expansions, $J - J_c \propto \lambda a$, or by exact results farther from J_c [12,13,18].

(3) By measuring $\tau(\Lambda)$ on real systems or MD simulations, one estimates D with our relation (21) and the numerical coefficient A corresponding to the appropriate lattice.

(4) From the knowledge of D and the appropriate choice of a (shorter than any relevant length scale above the molecular ones), one eventually deduces the real time step δt corresponding to a Monte Carlo step through $\delta t = a^2/(4D)$ in two dimensions.

In the model B context under consideration here, composition fluctuations dissipate through the diffusion of microscopic constituents. The present work can in principle be

extended to contexts where additional hydrodynamic effects are taken into account. This is discussed in detail, for example, in Refs. [20,23,24] in the context of biphasic lipid membranes, where the internal membrane dynamics can additionally be coupled to the 3D hydrodynamics of the surrounding solvent. Instead of the model B used here, one would need to appeal to the so-called models H or HC as discussed in these references. Relating large-scale dynamics to coarse-grained Ising-like model ones remains to be done in this more complex situation.

[1] I. Herbut, *A Modern Approach to Critical Phenomena* (Cambridge University Press, Cambridge, 2010).

[2] M. Seul and D. Andelman, Domain shapes and patterns: The phenomenology of modulated phases, Science **267**, 476 (1995).

[3] A. R. Honerkamp-Smith, P. Cicuta, M. D. Collins, S. L. Veatch, M. den Nijs, M. Schick, and S. L. Keller, Line tensions, correlation lengths, and critical exponents in lipid membranes near critical points, Biophys. J. **95**, 236 (2008).

[4] A. R. Honerkamp-Smith, S. L. Veatch, and S. L. Keller, An introduction to critical points for biophysicists; observations of compositional heterogeneity in lipid membranes, Biochim. Biophys. Acta: Biomembranes **1788**, 53 (2009).

[5] P. M. Chaikin and T. C. Lubensky, *Principles of Condensed Matter Physics* (Cambridge University Press, Cambridge, 1995).

[6] B. Partridge and C. F. Lee, Critical Motility-Induced Phase Separation Belongs to the Ising Universality Class, Phys. Rev. Lett. **123**, 068002 (2019).

[7] C. Maggi, M. Paoluzzi, A. Crisanti, E. Zaccarelli, and N. Gnan, Universality class of the motility-induced critical point in large scale off-lattice simulations of active particles, Soft Matter **17**, 3807 (2021).

[8] J. Cornet, N. Destainville, and M. Manghi, Domain formation in bicomponent vesicles induced by composition-curvature coupling, J. Chem. Phys. **152**, 244705 (2020).

[9] S. Zakany, S. Smirnov, and M. C. Milinkovitch, Lizard Skin Patterns and the Ising Model, Phys. Rev. Lett. **128**, 048102 (2022).

[10] M. Merle, L. Messio, and J. Mozziconacci, Turing-like patterns in an asymmetric dynamic Ising model, Phys. Rev. E **100**, 042111 (2019).

[11] Y.-P. Ma, I. Sudakov, C. Strong, and K. M. Golden, Ising model for melt ponds on Arctic sea ice, New J. Phys. **21**, 063029 (2019).

[12] J. E. Avron, S. H. van Beijeren, L. S. Schulman, and R. K. P. Zia, Roughening transition, surface tension and equilibrium droplet shapes in a two-dimensional Ising system, J. Phys. A: Math. Gen. **15**, L81 (1982).

[13] V. A. Shneidman and R. K. P. Zia, Wulff shapes and the critical nucleus for a triangular Ising lattice, Phys. Rev. B **63**, 085410 (2001).

[14] M. E. J. Newman and G. T. Barkema, *Monte Carlo Methods in Statistical Mechanics* (Clarendon Press, Oxford, 1999).

[15] A. J. Bray, Theory of phase-ordering kinetics, Adv. Phys. **43**, 357 (1994).

[16] C. Esposito, A. Tian, S. Melamed, C. Johnson, S. Y. Tee, T. Baumgart, Flicker spectroscopy of thermal lipid bilayer domain boundary fluctuations, Biophys. J. **93**, 3169 (2007).

[17] S. J. Marrink *et al.*, Computational modeling of realistic cell membranes, Chem. Rev. **119**, 6184 (2019).

[18] R. Baxter, *Exactly Solved Models in Statistical Mechanics* (Academic Press, London, 1982).

[19] B. A. Scalettar, J. R. Abney, and J. C. Owicki, Theoretical comparison of the self diffusion and mutual diffusion of interacting membrane proteins, Proc. Natl. Acad. Sci. USA **85**, 6726 (1988).

[20] A. Honerkamp-Smith, B. B. Matcha, and S. L. Keller, Experimental Observations of Dynamic Critical Phenomena in a Lipid Membrane, Phys. Rev. Lett. **108**, 265702 (2012).

[21] Y. Achiam, Diffusion in the one-dimensional Ising model, J. Phys. A: Math. Gen. **13**, 1825 (1980).

[22] S. L. Veatch, P. Cicuta, P. Sengupta, A. Honerkamp-Smith, D. Holowka, and B. Baird, Critical fluctuations in plasma membrane vesicles, ACS Chem. Biol. **3**, 287 (2008).

[23] B. A. Camley, C. Esposito, T. Baumgart, and F. L. H. Brown, Lipid bilayer domain fluctuations as a probe of membrane viscosity, Biophys. J. **99**, L44 (2010).

[24] B. A. Camley and F. L. H. Brown, Dynamic Simulations of Multicomponent Lipid Membranes over Long Length and Time Scales, Phys. Rev. Lett. **105**, 148102 (2010).